Cross-correlation and image alignment for multi-band IR sensors

Thomas Lu[1a], Tien-Hsin Chao[a], Kang (Frank) Chen[b], Andrew Luong[c], Mallory Dewees[d], Xinyi Yan[e], Edward Chow[a], and Gilbert Torres[f]

[a]Jet Propulsion Lab/California Institute of Technology, Pasadena, CA, USA;[b]Univ. Calif., Los Angeles, CA, USA, [c]Univ. Calif., Irvine, CA, USA, [d]Saddleback College, CA, USA, [e]Univ. Calif., Berkley, CA, USA, [f]Naval Air Warfare Center, Point Mugu, CA, USA

ABSTRACT

We present the development of a cross-correlation algorithm for correlating objects in the long wave, mid wave and short wave Infrared sensor arrays. The goal is to align the images in the multi-sensor suite by correlating multiple key features in the images. Due to the wavelength differences, the object appears very differently in the sensor images even the sensors focus on the same object. In order to perform accurate correlation of the same object in the multi-band images, we perform image processing on the images so that the features of the object become similar to each other. Fourier domain band pass filters are used to enhance the images. Mexican Hat and Gaussian Derivative Wavelets are used to further enhance the features of the object. A Python based QT graphical user interface has been implemented to carry out the process. We show reliable results of the cross-correlation of the objects in multiple band videos.

Keywords: Multi-band IR images, cross-correlation, image processing, feature extraction, Wavelets.

1. INTRODUCTION

Computer vision has been widely used in industrial automation, robotics, and image understanding. Correlation is one of the most important building blocks of computer vision [1]. Searching for a known object in an unknown image has been a research topic for many years. Although human eyes can do correlation quite easily and efficiently, it is still a difficult task for computer to match a pattern due to in plane scale, rotation, shift and out of plane perspective changes [2-5]. The background clutters around the object also pose challenges to the correlation operations in the computer vision. In this paper, we present an optimization process to correlate common features of the objects in multiple Infrared (IR) video images simultaneously. The videos were recorded by multiple IR sensors in three IR bands, longwave (LW), midwave (MW) and shortwave (SW). The sensors have different resolutions. They are not calibrated. The object looks similar in different IR bands, but they have many different features. They are not aligned in the videos. The background has noise and clutters. Our goal is to enhance the object in each IR band, track and align the object in the sensor videos, then segment the object from the background. We will focus on the correlation and geometric transformation operations in this paper. Fourier transform is widely used in image analysis and processing. We apply a number of Fourier domain filtering methods to enhance the features and reduce the background clutters. The FFT can be implemented in parallel processors such as the GPUs for high-speed operations [6]. In fact, an optical lens can perform a perfect complex Fourier transform [7]. Many optical correlators have been built to perform the correlation operations. JPL has built a compact optical correlator that is only 2"x2"x2" in its optical path [8]. It is capable of performing up to 1000 image correlations per second in HD format [9].

[1] Contact e-mail: Thomas.t.lu@jpl.nasa.gov

Optical Pattern Recognition XXVII, edited by David Casasent, Mohammad S. Alam, Proc. of SPIE
Vol. 9845, 984505 · © 2016 SPIE · CCC code: 0277-786X/16/$18 · doi: 10.1117/12.2224694

In Section 2, we discuss the correlation operation. Since the IR images contain low resolution objects, in Section 3, we discuss the Sobel filter to enhance the edges of the multi-band IR images. In Section 4 and 5, we further expand the pre-processing operations of the IR images using the Mexican-Hat Wavelet and the Derivative of Gaussian filters. We present the geometric transformation of the multiple IR sensor images in Section 6. In Section 7, we analyze the test results.

2. CROSS-CORRELATION

Correlation is an effective process to match similar features in two different images. The two-dimensional discrete cross correlation of a template g and an image f can be expressed in the following formula [7]:

$$c_{ij} = \frac{\sum_m \sum_n [f(m+i,n+j)-f'][g(m,n)-g']}{\sqrt{\sum_m \sum_n [f(m,n)-f']^2 [g(m,n)-g']^2}}; \quad (1)$$

where c_{ij} is the correlation value at pixel location (i, j), f' and g' are the mean values of the image f and template g, respectively.

In many cases, the correlation can be carried out in the Fourier domain to take advantage of the fast Fourier transform (FFT) operations.

$$F = \mathcal{F}\{ f \}, G = \mathcal{F}\{ g \}; \quad (2)$$

where $\mathcal{F}$ represent the Fourier transform operation. Then the correlation function in Fourier domain becomes

$$C = F \circ G^*, \; c = \mathcal{F}^{-1}\{ C \}; \quad (3)$$

where $\circ$ represents the entry wise product of the F and G matrices, and * is the complex conjugate operation. $\mathcal{F}^{-1}$ represents the inverse Fourier transform.

To find if there is any part in image f that is of any resemblance of the template g, one can look for any correlation peaks in the correlation plane C. Then the correlation peak can be expressed as:

$$P(x,y) = \underbrace{argmax}_{(i,j)} \{c\}; \quad (4)$$

where P represents the peaks or local maximum points in the correlation plane. The higher and sharper the peak, the higher similarity are between the template g and the pattern in the image f.

3. MEXICAN HAT WAVELET FILTER

Aside from the intrinsic calibration differences between the single band sensors, the qualities and features detected by the shortwave sensors were fundamentally different from the LW sensors. Far more detail was present in the SW images than in the LW and details of the objects including paint markings and glare were more enhanced. Background noise was also enhanced and became prominent features in the images. In order to facilitate correlation between the shortwave and LW, this extra detail present in the shortwave images had to be suppressed.

Using a wavelet based filter seemed appropriate as a preprocessing method as it offered some amount of control over the qualities of the features enhanced. [10-11] The filter utilizes a continuous wavelet transform, which is a Fourier transform based analysis. [12] Like a Fourier transform, it analyzes the similarity between a signal and a particular function. However, the continuous wavelet transform constitutes a scale space representation of the image data and can consequently be used to filter an image for features of a certain size.

The wavelet transform's strength is rooted in this ability be scaled according to the resolution of detail desired. Where using a short time Fourier transform results in a fixed window of analysis, the wavelet transform is windowed according to the spatial frequency encountered within an image. The higher the scale of the wavelet the smaller the filter window. Also, by stretching, compressing and shifting the localized wavelet accordingly, features ranging from minute to predominant will be isolated. More compression will correlate with finer detail. Much as a trigonometric function can be stretched and compressed by scaling its argument by a factor, so can a wavelet. The greater the scaling factor the larger the features detected in an image will be. The generation of the continuous wavelet transform by inverse Fourier transforms is permitted by this relationship. Scaling the wavelet so that a certain scale feature will be enhanced provides a corresponding frequency to be filtered for. This allows for the generation of a band-pass filter. [13]

The scaling factors within the wavelet functions therefore provide inherent parameters for methods designed to filter images. The wavelet chosen for the transform was the Mexican hat wavelet, a wavelet in the derivative of Gaussian wavelet family, as it is non-directional and therefore can detect image features in all orientations.

The Mexican Hat wavelet function in one dimension, provided by Matlab, as depicted in Figure 1 is represented by

$$\varphi(x) = \frac{2}{\sqrt{3\sigma}\pi^{\frac{1}{4}}}\left(1 - \frac{x^2}{\sigma^2}\right)e^{-\frac{x^2}{2\sigma^2}}; \tag{5}$$

where σ is the scaling factor. The below figure visualizes this function at two scales.

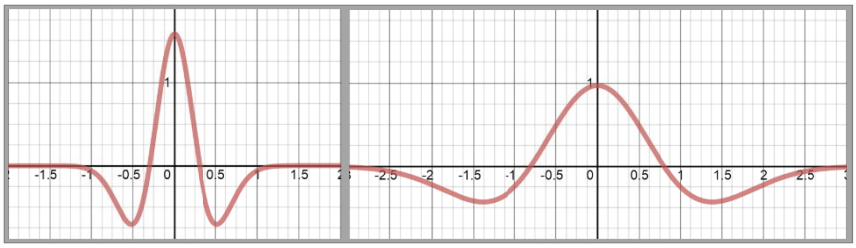

Figure 1: Mexican hat wavelet function in one dimension with scaling factor σ adjusted to .3 and .8 respectively.

The Mexican hat wavelet transform equation used to process the images, provided by Matlab, in two dimensions (see Figure 2) is represented by

$$\varphi(\omega_x, \omega_y)) = -2\pi\left({\omega_x}^2 + {\omega_y}^2\right)^{p/2} e^{-\frac{[(\sigma_x\omega_x)^2 + (\sigma_y\omega_y)^2]}{2}} \quad \sigma_x \in R, \sigma_y \in R, p > 0; \tag{6}$$

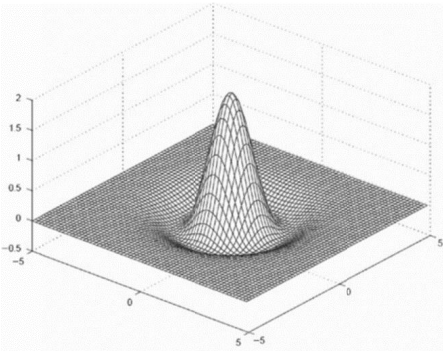

where the scale is manipulated by the factors σ_x and σ_y. A three dimensional viewpoint of the graph of this function in two variables is depicted in Figure 2. Although the scalability of this transform allows for greater flexibility in resolution enhancement, inherent differences in the images including the dimension in pixels of the object to be enhanced caused optimization of the method for all cases to be difficult. An example of the different scaling factors on the images is displayed in Figure 3.

Figure 2: Graphical Representation of the two dimensional Mexican Hat wavelet function, courtesy of "Signal and Multi-resolution Analysis-Chapter 1" by Abdelialil Quahabi

The continuous wavelet transformation results in a coefficient matrix where each coefficient is a function of scale and position. These coefficients denote the similarity between the image characteristics at an image location and the wavelet function at a certain scale. Points exhibiting high similarity to the wavelet will correspond to coefficients of greater magnitude. A reconstruction of the image can be acquired from these coefficients. For the purposes of this project, the plot of the coefficient matrix created when the wavelet is scaled appropriately for the desired features provided an ideal rendering of the image for use in detecting edges. Application of linear averaging filters or Sobel filters to this coefficient matrix could then be utilized to enhance the edges of the aircraft.

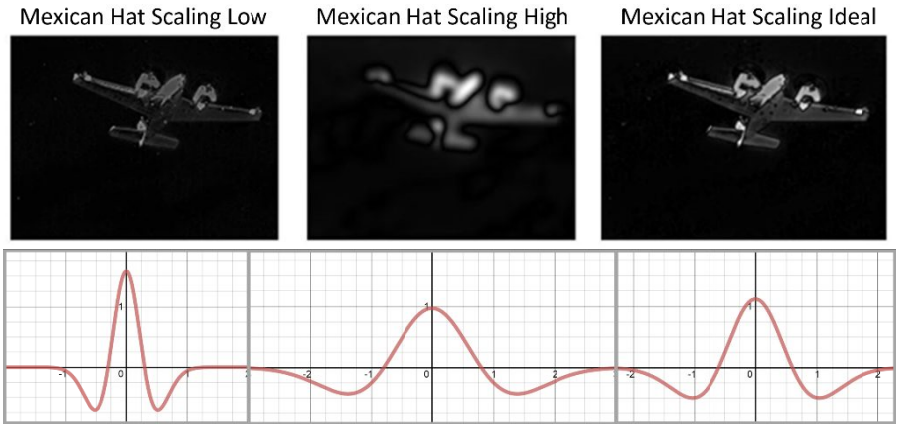

Figure 3: This image demonstrates the effect of scaling the sigma-x and sigma-y parameters in the above 2-D transformation function when pre-processing image. The upper row shows the effect of the image. The second row shows the effect of adjusting a similar parameter on the 1-D function.

4. GAUSSIAN DERIVATIVE FILTER

Gaussian filter in Fourier domain is an effective feature detection method for image processing. Figure 4(a) shows a 2D Gaussian filter. It is a low-pass filter that can effectively reduce the background noise. If we want to enhance the high frequency part of the image, the inverse Gaussian filter can be applied, as shown in Figure 4(b). A Gaussian filter can be expressed in Eq. (7).

$$G_\sigma(x,y) = \frac{1}{2\pi\sigma^2} e^{-\frac{x^2+y^2}{2\sigma^2}}; \quad (7)$$

where σ is the scaling factor.

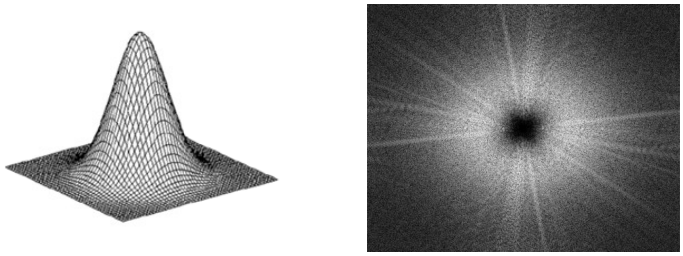

(a) (b)

Figure 4: (a) Shape of a 2D Gaussian filter, (b) Intensity map of an inverse of Gaussian filter in Fourier domain.

In order to effectively enhance the edges of the objects in the LW image and suppress the background, we have designed a filter that combines a Gaussian derivative filter with an inverse Gaussian derivative filter. This filter can be represented by the Eq. (8) below.

$$\frac{\partial G_\sigma(x,y)}{\partial x} \propto xe^{-\frac{x^2+y^2}{2\sigma^2}}, \quad \frac{\partial G_\sigma(x,y)}{\partial y} \propto ye^{-\frac{x^2+y^2}{2\sigma^2}}, \quad \nabla G_\sigma = [\frac{\partial G_\sigma}{\partial x}\frac{\partial G_\sigma}{\partial y}]^t ; \tag{8}$$

A 2D plot of the Gaussian derivative filter is illustrated in Figure 5(a). It enables to enhance the edges in the Y-axis direction. By rotating the Gaussian derivative filter matrix clockwise 90 degree, it enhances the edges in the X-axis direction. When we use the absolute values of the resulting images, both the positive and negative edges can be enhanced at the same time, as shown in Figure 5(b).

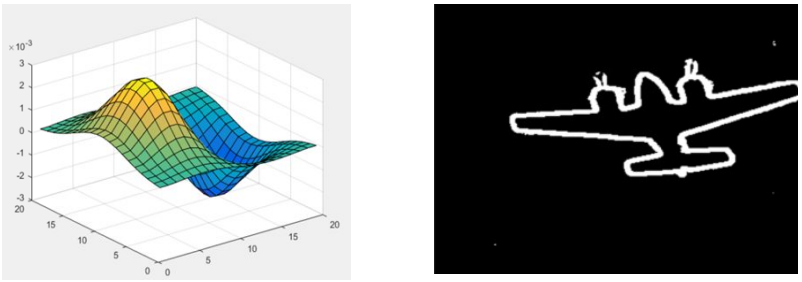

(a) (b)

Figure 5: (a) Shape of the derivative Gaussian filter, and (b) the results of edge enhancement.

5. OPTIMIZATION OF CORRELATION OPERATIONS

The key features in the IR images are quite simple and similar to each other. A wrong correlation peak in another location could be higher than the correct one, resulting incorrect identification of the key features. In order to make the correlation operations more robust, we have implemented localized correlation and peak-to-sidelobe ratio (PSR) optimization.

5.1 Localized Correlation

After the preprocessing using the wavelet filters, we pick several key features in an IR band to be cross-correlated to another band, and to be self-correlated to the next frame in the same IR band. Figure 6(a) shows a SW image. Four points were picked to be the key features (Green dots). A template cut out from a key feature of another IR band is displayed in Figure 7(b). It scans through the entire image to match the similar feature. Figure 7(c) shows the 3D plot of the correlation plane. The highest peak in the correlation plane is chosen as the most likely matching feature between the two bands.

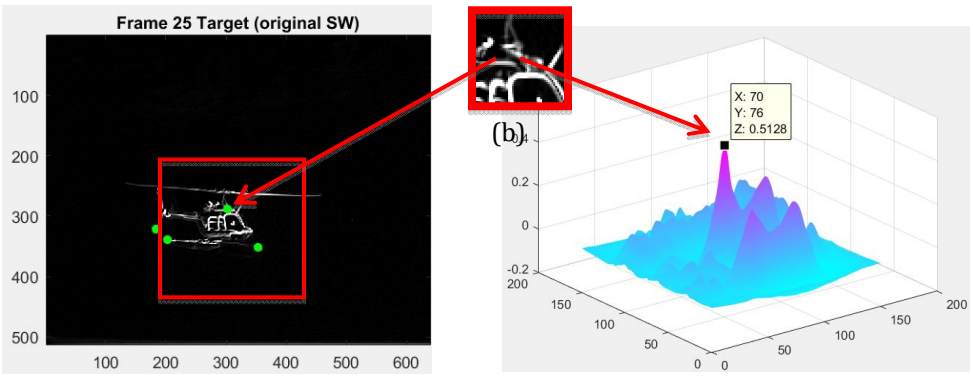

Figure 6: Localized correlation: (a) target image and search area (red square), (b) template of a target feature; (c) 3D plot of the correlation plane.

We have implemented a localized correlation method to limit the search of a 50x50 pixels template in an area of 100x100 pixels window instead of searching the entire image plane. Since the corresponding features in the wave bands are located close to each other, the localized correlation results in reduced error and faster processing speed.

5.2 Coarse and Fine Search

In many cases, some moving parts such as rotors were in the correlation windows, which cause drifts or jumps of the correlation peaks. In order to exclude any moving parts, we further reduce the template size from 50x50 pixels to 5x5 pixels and implemented a two-step search strategy. As shown in Figure 7, in the coarse search step, a 50x50 pixels template searches in a 100x100 pixels window for a correlation peak. In the fine search step, we reduce the template size to 5x5 pixels and search in a 15x15 pixels window. We then make an average of the two correlation peak positions as our final peak position in this image.

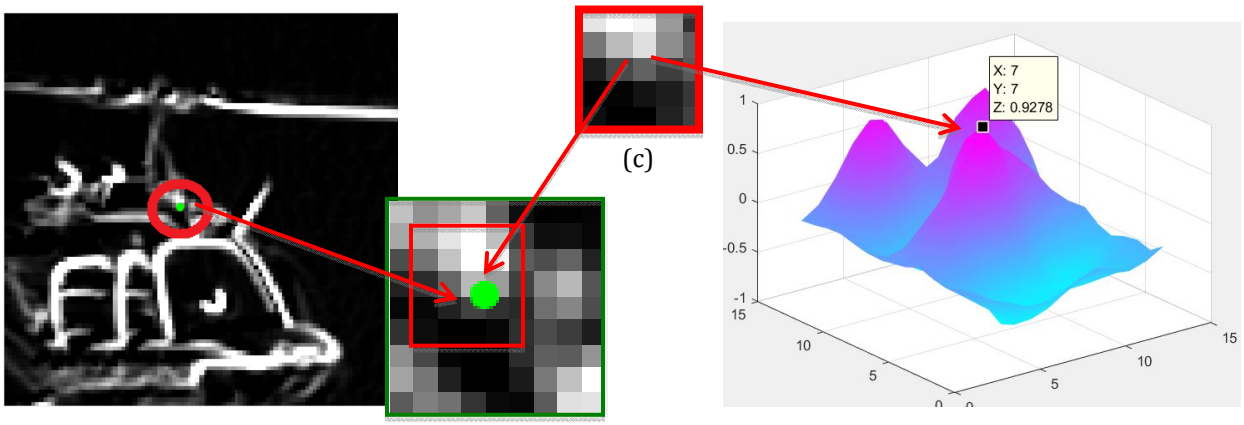

Figure 7: Coarse and fine search in the correlation: (a) target image, (b) coarse search template, (c) fine search template, (d) fine search correlation peak.

5.3 Peak-to-Sidelobe Ratio Optimization

Many IR features are similar to each other; picking the highest peak value in the correlation plane may not always be the correct result. We need additional criteria to distinguish the true correlation peak against the false peaks.

The peak-to-sidelobe ratio (PSR) is defined as the ratio between the peak area intensity and the surrounding area intensity. It defines the quality of a peak, i.e., high PSR value means that the peak is sharp, which in turn, means that the two features are highly correlated. A low PSR means that the features are not correlated well. The PSR helps to eliminate the correlation peaks that have high intensity values but the peak widths are broad.

The distance between the previous known feature point to the new correlation peak can be a good indicator, too. We prefer to pick the peak closer to the original point. Therefore, the peak distance is used in the peak selection equation. Eq. (9) shows the general peak selection criteria PSR Prime (PSR'):

$$PSR' = \alpha*PSR - \beta*Distance + \gamma*Peak; \quad (9)$$

where α, β, and γ are the weights for the PSR value, the peak distance, and the peak intensity value, respectively.

Figure 7 shows the performances of the different criteria. Total 40 peaks were used to Compare the accuracy of identifying true correlation peaks using three criteria: PSR', peak intensity only, and PSR value only. PSR' can identify 39 peaks correctly, while peak only method only identified 32 peaks, and the PSR only method identified 21 peak out of 40 peaks. The PSR' is a clear winner in identifying the true correlation peak in the correlation plane.

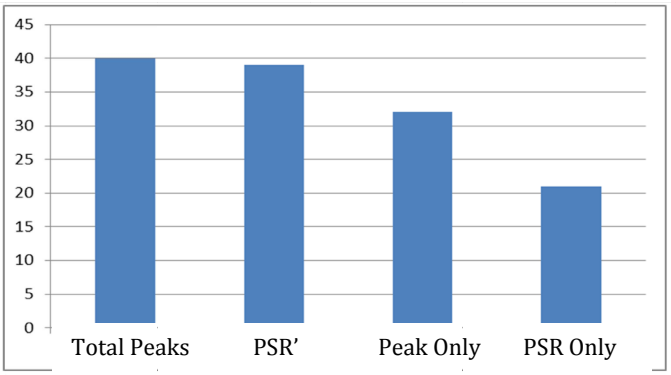

Figure 8: Total 40 peaks were used to Compare the accuracy of identifying true correlation peaks using three criteria: PSR', peak intensity only, and PSR value only.

6. IMAGE REGISTRATION

Once the key features are correlated between the LW, MW and SW images, they can calibrate and align the target based on the correlation points using an image registration method. Image registration is the process of aligning to or more images of the same object. It involves performing geometric transformations on the moving images to align them to the fixed image. We want to perform image registration because, although the different wavelength images are of the same object, the camera setup may have been slightly different for each set, and therefore cause the object to have slightly different position, scale, and rotation. Registering the LW, MW and SW images together accurately simplifies the segmentation process by allowing us to use a single segmentation mask to segment the three sets of images instead of individually segmenting each wavelength.

The three geometric transformations we were interested in, based on our data, were translation, rotation, and scaling. Translation is the geometric transformation that shifts every point in the figure or image in the same direction and distance. Rotation is a geometric transformation that rotates the figure or image about the center by a set angle. Scaling creates an image that is similar to the original image except for the difference in

size. The transformation matrices are illustrated in Table 1. We are really only interested in these three geometric transformations because our test data is generally taken the same way within each test case, besides some differences in camera calibration, which a translation, rotation, or scaling can fix.

Table 1: Affine geometric transformation matrices work.

Transform	Transformation Matrix	Description
Translation	$\begin{matrix} 1 & 0 & 0 \\ 0 & 1 & 0 \\ Tx & Ty & 1 \end{matrix}$	Tx is the shift in the x dimension Ty is the shift in the y dimension
Scale	$\begin{matrix} Sx & 0 & 0 \\ 0 & Sy & 0 \\ 0 & 0 & 1 \end{matrix}$	Sx is the scale factor in the x dimension Sy is the scale factor in the y dimension
Rotation	$\begin{matrix} \cos(q) & \sin(q) & 0 \\ -\sin(q) & \cos(q) & 0 \\ 0 & 0 & 1 \end{matrix}$	q is the angle of rotation

The first method we tried to use was fairly simple. After the correlation process was done and we had a set of feature points for each set of images, we used the built-in Matlab function fitgeotrans to create a Matlab tform object that is used to transform the moving images (SW and MW) to align it with the fixed image (LW). More specifically, the fitgeotrans function takes in a set of fixed points, a set of moving points, and a type of transformation, and outputs a 3x3 transformation matrix that is applied to the moving images. One thing to note is that the geometric transformations that are calculated into the transformation matrix are translation, rotation, scale, and shear.

Although the resulting overlay/ alignment was fairly accurate using the method above, it was heavily reliant on a very accurate correlation. If the feature points in the correlation was slightly off for a few pixels, even if only by 5-10 pixels, the transformation will become skewed and inaccurate. In Figure 9(a) below, one point's coordinates were changed to be slightly off from the point of interest to show the effects of a slightly inaccurate correlation on the registration.

The second method of transformation that we implemented sought to make the registration and transformation process more stable. Instead of using the built-in function fitgeotrans, the translation, rotation, and scale was calculated separately and we used these values to create the 3x3 transformation matrix. Unlike the first method, this method currently does not have a shear calculation implemented.

To find the necessary x and y shift for the fixed and moving images to be in the same position, we take difference in the x coordinates between the fixed image and moving image of the current frame, and average all of those differences to calculate the x shift. The same thing is done to the y-dimension to calculate the y shift. One thing that needs to be done before calculating the shift is apply the rotation and scaling changes to the feature points' coordinates. If the coordinates are not transformed, they will not match up to the images after the scaling and rotation is done and the shift will be inaccurate.

To calculate the scaling that is needed to make the objects in the image the same size, we calculate a scaling ratio using distances. We calculate the distance from point 1 to point 2 on the fixed image, calculate the distance from point 1 to point 2 on the moving image, and the ratio between those two distances is the scaling ratio that is applied to the moving image of that frame.

To find the rotation, the difference in angle between two lines in the images is calculated. The slope from point 1 to point 2 is found in both the moving and fixed images. The difference in angle between those two lines, and subsequently the two images, is the difference between the inverse tangent of the fixed slope and inverse tangent of the moving slope.

Two things were done to make the transformation calculations more stable: use more points in the calculation of the rotation and scale, and average the scaling ratio and angle of rotation with the previous frame and next frame. For scale and rotation respectively, instead of calculating the distance and slope of point 1 to point two, we calculate the distance and slope from each point to every other point. By doing this, the results are more normalized, even if one or more points from the correlation are inaccurate.

Figure 9 shows the side-by-side comparison of a test case for image registration. Current method (Figure 9(b)) does not have extreme shear problem. One point from the correlation is purposely shifted over 20 pixels. Image 9(a) has the tail of the helicopter slightly misaligned where 9(b) is still basically an accurate overlay. Overall, this method produces similarly accurate results to the initial method, even if there is a slightly fewer number accurate feature points for the current frame. And because there is averaging of the rotation, scaling, and shifting calculations, the transformation matrix is less likely to become inaccurate because of outliers in the correlation.

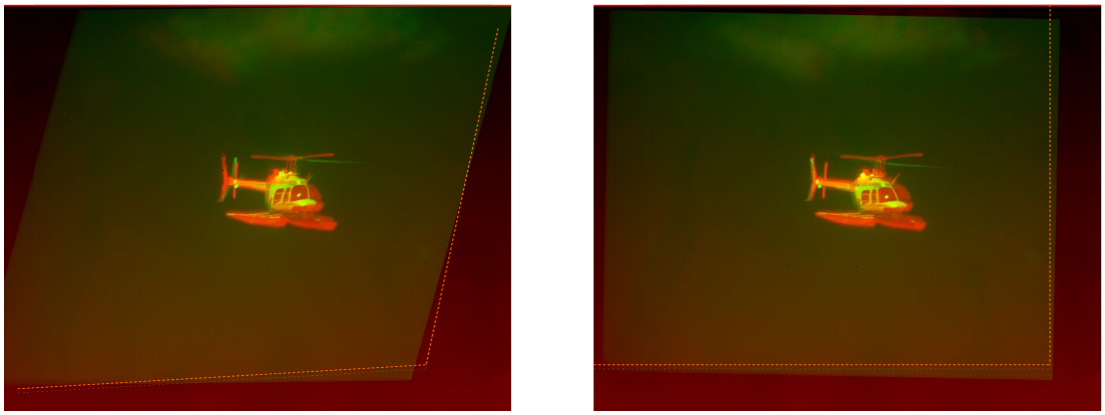

(a) (b)

Figure 9: Comparison of registration between initial and current methods. (a) using Matlab function; (b) performing translation, rotation and scale separately.

7. EXPERIMENTAL RESULTS AND ANALYSIS

We have tested and compared the performance of the correlation strategies with Wavelet and Sobel filters using 5 test cases. Each test case contains 3 videos, i.e., LW, MW, and SW videos. A segment of 50 frames were selected from each video. A total of 750 frames were used in the test run.

First an accurate standard feature coordinate is established for each test video. An automatic frame by frame correlation was run first to determine the feature coordinates. Then we manually check the accuracy of the coordinates and correct the erroneous coordinates to ensure accurate feature coordinates in each frame.

Secondly, a test program was implemented that runs different pre-processing methods in combination with the correlation. We have used 4 types of pre-processing filters in our algorithm:

(1) No filter,
(2) Wavelet filter,
(3) Sobel filter, and
(4) Wavelet + Sobel filter.

Thirdly, three correlation strategies were run to compare the performance:

1. **Cross-Correlation** – Cross-correlation between LW to MW and MW to SW on every frame of the video.

2. **Self-Correlation** – Self-correlation between the neighboring frames within each wave band.
3. **Cross + Self-Correlation** – Cross correlation between LW to MW and MW to SW only on the first frame, then run self-correlation on the rest of the frames within each wave band.

Figure 10 shows the performance comparison of the 3 correlation strategies using 4 different pre-processing filters. The first bar (Blue vertical pattern) represents the Cross-Correlation, the second (Red back slanted pattern) Self-Correlation, and the third (Green forward slanted pattern) Cross + Self-Correlation. The three correlation strategies are further separated into 4 groups, which represent 4 pre-processing filters: "No filter", "Wavelet", "Sobel", and "Wavelet+Sobel".

The Y-Axis represents the relative distance, i.e., pixel error, between the resulting feature coordinates and the standard coordinates. From the figure we can see that the pixel errors for the correlations without and pre-processing filter (No filter) are the greatest, between 17.27 pixels to 43.55 pixels. The Wavelet+Sobel pre-processing filter combination gives the best performance, only 4.33 pixels error for the Self-Correlation, 5.45 pixels error for the Cross+Self-Correlation, and 15.64 pixels error for the Cross-Correlation.

The Self-Correlation within each wave band usually performs accurate correlation because the features between neighboring frames are generally very similar to each other. By using the Wavelet+Sobel filter, the average pixel error reduced from 17.27 pixels to 4.33 pixels, a 75% reduction in error!

The Cross-Correlation is more difficult because the target features between LW to MW, and MW to SW are generally quite different, making cross-correlation very challenging. Without a filter, the average pixel error is 29.81 pixels. With a Wavelet filter, the average pixel error reduced to 11.70 pixels, around 60% improvement.

The Cross+Self Correlation effectively tracks the target features between bands and within a band. However, the average pixel error is very high without using any filter, 43.55 pixels. By using a Wavelet+Sobel filter, the average pixel error is reduced to 5.45 pixels, an 87% improvement!

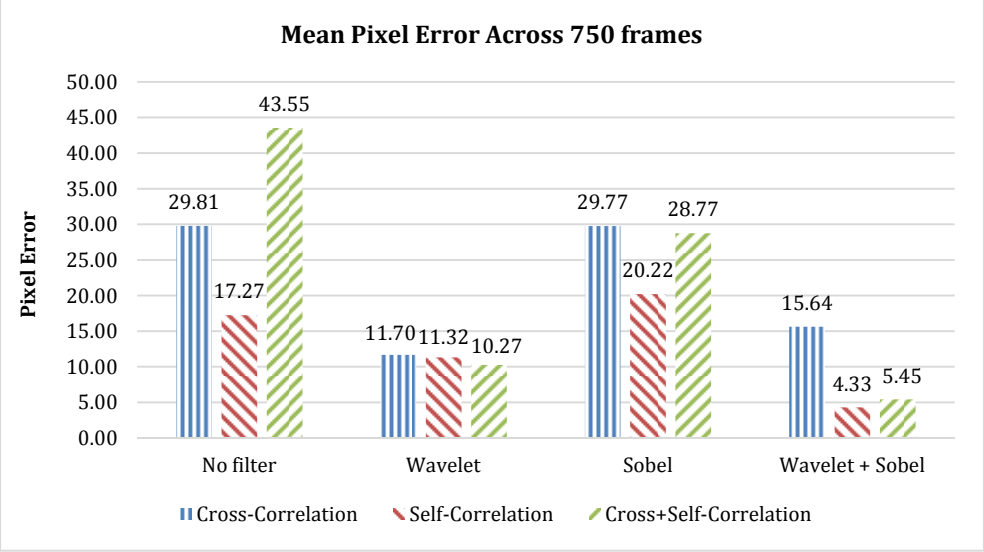

Figure 10: Performance comparison of three correlation strategies using four different pre-processing filters.

5. CONCLUSIONS

We have shown several correlation strategies for target feature identification and tracking in multiple IR wave bands. Due to low resolution and distortion in the IR images, the correlation operations would generate high error if performed without pre-processing. By using a combination of the optimized Mexican Hat Wavelet and Sobel filters as the pre-processing for the self- and cross-correlation, the average error for tracking the target features has been reduced up to 87%. Further improvement of the correlation accuracy can be obtained by optimizing the custom linear filters.

6. ACKNOWLEDGEMENTS

The research described in this paper was carried out at the Jet Propulsion Laboratory, California Institute of Technology and was supported in part by the U.S. Department of Defense, Test Resource Management Center, Test & Evaluation/Science and Technology (T&E/S&T) Program under NASA prime contract NAS7-03001, Task Plan Number 81-12346. We acknowledge Kevin De Jesus, Nicole Backer, and Franklin Heng for their contributions in testing the correlation and PSR algorithms.

REFERENCES

[1] Lu, T., C. L. Hughlett, H. Zhou, T-H. Chao, J. C. Hanan, "Neural network post-processing of grayscale optical correlator," Proc. *SPIE* 5908, *Optical Information Processing III*, (2005).
[2] Casasent, D., D. Psaltis, "New optical transforms for pattern recognition," Proc. IEEE 65, 77-84 (1977).
[3] Yang, Y., Hsu, Y. N., and H. H. Arsenault, "Optimum circular filters and their uses in optical pattern recognition," Opt. Acta 29, 627-644 (1982).
[4] Schils, G. F., D. W. Sweeney, "Rotationally invariant correlation filtering," J. Opt. Soc. Am. A 2, 1411-1418 (1985).
[5] Casasent, D., M. Krauss, "Polar camera for space-variant pattern recognition," Appl. Opt. 17, 1559-1561 (1978).
[6] Caulfield, H. J., M. H. Weinberg, "Computer recognition of 2-D patterns using generalized matched filters," Appl. Opt. 21, 1699-1704 (1982).
[7] Chao, T-H., G. Reyes, Y. Park, "Grayscale Optical Correlator", SPIE v.3386 (1998).
[8] Zhou, H., C. L. Hughlett, J. C. Hanan, T. Lu, T-H. Chao. "Development of streamlined OT-MACH-based ATR algorithm for grayscale optical correlator," p. 78-83, *Optical Pattern Recognition XVI; SPIE* **5816** (2005).
[9] Chao, T-H and Lu, T., "High-speed Optical Correlator with Custom Electronics Interface Design," SPIE Proc. Vol. 8748 (2013).
[10] Tan, L., Ma, J., Wang, Q., and Ran, Q., "Filtering Theory and Application of Wavelet Optics at the Spatial- Frequency Domain," Appl. Opt. 40, 257-260, (2001)
[11] Chiang J., Y. Zhang, Lu, T., T-H. Chao, "Composite Wavelet Filters for Enhanced Automatic Target Recognition," SPIE Optical Pattern Recognition XXIII, Vol. 8298 (2012).
[12] The Mathworks Inc, "Continuous Wavelet Transform and Scale Based Analysis," 2016, Retrieved from http://www.mathworks.com
[13] The Mathworks Inc, "Continuous Wavelet Transform as a Bandpass Filter," 2016, Retrieved from http://www.mathworks.com
[14] Lu, T., and Mintzer, D., "Hybrid neural networks for nonlinear pattern recognition," Optical Pattern Recognition, ed. by F. T. S. Yu & S. Jutamulia, Cambridge University Press, (1998).

[15] Lin, T., Lu, T., Braun, H., Edens, W., Zhang, Y., Chao, T-H., Assad, C., and Huntsberger, T., "Optimization of a multi-stage ATR system for small target identification," Proc. SPIE, 7696 (2010).
[16] W. Nicholas Greene, Yuhan Zhang, T. Lu , T-H. Chao, "Feature extraction and selection strategies for automated target recognition," SPIE Symposium on Defense, Security & Sensing Conference, Independent Component Analyses, Wavelets, Neural Networks, Biosystems, and Nanoengineering, Proceedings of SPIE Vol. 7703 (2010).
[17] Johnson, O., Edens, W., Lu, T., Chao, T. "Optimization of OT-MACH filter generation for target recognition," Optical Pattern Recognition XX. Proceedings of the SPIE, Volume 7340 (2009).
[18] Williams, Stephen and Lu, T., "Visual target tracking in the presence of unknown observer motion," Proc. SPIE, Vol. 7340 -11, Optical Pattern Recognition XX. (2009).